Coordinated V-f and P-Q Control of Solar Photovoltaic Generators With MPPT and Battery Storage in Microgrids

Sarina Adhikari, *Student Member, IEEE*, and Fangxing Li, *Senior Member, IEEE*

Abstract—The microgrid concept allows small distributed energy resources (DERs) to act in a coordinated manner to provide a necessary amount of active power and ancillary service when required. This paper proposes an approach of coordinated and integrated control of solar PV generators with the maximum power point tracking (MPPT) control and battery storage control to provide voltage and frequency (V-f) support to an islanded microgrid. Also, active and nonactive/reactive power (P-Q) control with solar PV, MPPT and battery storage is proposed for the grid connected mode. The control strategies show effective coordination between inverter V-f (or P-Q) control, MPPT control, and energy storage charging and discharging control. The paper also shows an effective coordination among participating microresources while considering the case of changing irradiance and battery state of charge (SOC) constraint. The simulation studies are carried out with the IEEE 13-bus feeder test system in grid connected and islanded microgrid modes. The results clearly verify the effectiveness of proposed control methods. The simulations are carried out in Matlab and Simpowersystems.

Index Terms—Active and reactive power control, distributed energy resource (DER), distributed generation (DG), maximum power point tracking (MPPT), voltage and frequency control, solar photovoltaic (PV).

I. NOMENCLATURE

$v_t(t)$	Instantaneous PCC voltage
$V_t(t)$	Average PCC voltage
$v_c(t)$	Instantaneous inverter output voltage
$V_c(t)$	Average inverter output voltage
L_c	Coupling inductor
P(t)	Inverter average active power
Q(t)	Inverter average reactive power
S(t)	Inverter average apparent power
δ^*	Duty cycle of DC/DC booster
P_{MPPref}	Reference maximum power
P_{PV}	PV active power output
α_1^*	Phase shift between $v_c(t)$ and $v_t(t)$
f_{ref}	Reference microgrid frequency
f_{measured}	Measured microgrid frequency
P_{AC}	AC side total average active power
P_{DC}	DC side average active power
P_{Battref}	Reference battery active power
P_{Batt}	Actual injected battery active power
Q_{ref}	Average reactive power reference (Reactive load)
Q_{actual}	Actual generated reactive power
P_{ref}	Average active power reference (Active load)
P_{actual}	Actual generated active power

II. INTRODUCTION

THE microgrid is a collection of distributed generators or microresources, energy storage devices, and loads which operate as a single and independent controllable system capable of providing both power and heat to the area of service [1]. The microresources that are incorporated in a microgrid are comprised of small units, less than 100 kW, provided with power electronics (PE) interface. Most common resources are Solar Photovoltaic (PV), Fuel Cell (FC), or microturbines connected at the distribution voltage level.

In a microgrid, the microsources and storage devices are connected to the feeders through the microsource controllers (MCs) and the coordination among the microsources is carried out by the central controller (CC) [2]. The microgrid is connected to the medium voltage level utility grid at the point of common coupling (PCC) through the circuit breakers. When a microgrid is connected to the grid, the operational control of voltage and frequency is done entirely by the grid; however, a microgrid still supplies the critical loads at PCC, thus, acting as a PQ bus. In islanded condition, a microgrid has to operate on its own, independent of the grid, to control the voltage and frequency of the microgrid and hence, acts like a PV (power-voltage) bus. The

operation and management in both the modes is controlled and coordinated with the help of microsource controllers (MCs) at the local level and central controller (CCs) at the global level.

Similar to the traditional synchronous generator frequency control [3], the microgrid voltage and frequency control can also be performed using droop control methods [4]–[8]. The present work provides fast response characteristics for voltage and frequency control as compared to the secondary control considered in [8]. The analogy between inverter control and the synchronous generator control in an islanded microgrid is studied in detail in [9]. In the islanded mode, there is the necessity of having a reference voltage and frequency signals in the microgrid inverter control [10].

The operation and control of the inverter interface of renewable-based distributed energy resources (DERs), like Solar Photovoltaic (PV) in a microgrid, is a real challenge, especially when it comes to maintaining both microgrid voltage and frequency within an acceptable range. A voltage control method based on traditional droop control for voltage sag mitigation along with voltage ride through capability is proposed in [11]. A dynamic voltage regulation based on adaptive control is proposed in [12], [13]. However, there are not many research works performed on V-f or P-Q control using solar PV including MPPT control and battery storage in microgrids. In [14], frequency regulation with PV in microgrids is studied; however, this work does not consider the voltage control objective and lacks battery storage in the microgrid.

In [15], a small scale PV is considered in a grid-connected mode to control the active and reactive power of the system. Here, the control methods consider abc-dq0 transformation and vice versa which is avoided in the present paper. In [16], power modulation of solar PV generators with an electric double layer capacitor as energy storage is considered for frequency control. In [17], load frequency control is implemented in microgrid with PV and storage; however, this work also lacks the consideration of a voltage control objective. The voltage and frequency control with solar PV and battery in microgrid with an induction machine is investigated in [18]; however, this work does not explain the transfer mechanism of controls to consider the battery SOC constraint. In summary, the previous works in this topic either lack the incorporation of an energy storage component or the voltage control objective along with frequency control or the incorporation of control transition in different scenarios. The present work fulfills these gaps by considering all of these objectives.

This paper proposes several control algorithms through which the capability of PV generators for voltage and frequency (V-f) control and active and nonactive/reactive power (P-Q) control in islanded and grid connected microgrids could be harnessed. Detailed models of PV, battery, inverter and converter are considered for the study. The major contribution and novelty of the proposed control methods lie in the coordination among individual proposed control methods: MPPT control at the PV side, battery control, and V-f/P-Q control algorithm at the inverter side. These three control algorithms at three stages are jointly linked through a power balance objective at the DC and AC side of the inverter so that the DC side voltage is indirectly controlled at the desired value in order
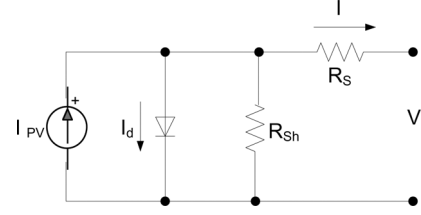

Fig. 1.   One diode equivalent circuit of Solar PV.

to maintain the AC side voltage at the utility desired voltage. Also, the proposed control methods have the capability of handling battery state of charge (SOC) constraints through the coordination of controls between participating microresources in the microgrid. This is a very important contribution from this work as compared to other literatures in this area. At the same time, the controls can seamlessly transform from one mode e.g., inverter P-Q control in grid connected mode to V-f control in islanded mode. The proposed control methods are validated with satisfactory results. The controls are developed in abc reference frames using the RMS/average values of voltages and active and reactive power. Hence, it is easy and efficient to implement, and avoids the transformation to and from other reference frames which greatly simplifies the control strategies. The chosen control parameters in the proposed methodologies are, however, dependent on the PV, battery, and external power grid conditions. These parameters can be adaptively achieved with the changing system conditions which could be a very promising future direction of this work.

The rest of the paper is organized as follows: Section III briefly presents the analytical modeling of Solar PV with model validation results. Section IV shows the PV system configuration, describes the modeling of the battery storage, and provides information about the structure of IEEE 13-bus distribution feeder under study. Section V describes the proposed coordinated V-f and P-Q control algorithms while incorporating PV MPPT control and battery storage control. Section VI presents convincing results to prove the effectiveness of the proposed control algorithms. Finally, Section VII summarizes the major contributions of the paper.

III. Solar PV Modeling and Validation

The commonly accepted solar cell model is a one diode model [19]. This work uses the single diode model of the solar cell to model the Kyocera KC200GT solar array, which is shown in Fig. 1.

The I-V characteristics of a solar array, as shown in Fig. 2, are represented by (1).

$$I = I_{\mathrm{PV}} - I_0 \left[\exp\left(\frac{V + R_s I}{V_{\mathrm{therm}} a} \right) - 1 \right] - \frac{V + R_s I}{R_{\mathrm{sh}}} \quad (1)$$

where I_{PV} and I_o are the photo current and the diode saturation currents, respectively; V_{therm} $(= N_s k T / q)$ is the thermal voltage of the array, N_s being the cells connected in series for greater output voltage, k is the Boltzmann constant $(1.3806503 \times 10^{-23}$ J/K), T (Kelvin) is the temperature of the p-n junction of the diode, and q $(1.60217646 \times 10^{-19}$C) is the electron charge; R_s and R_{sh} are the equivalent series and shunt resistances of the array, respectively; and a is the
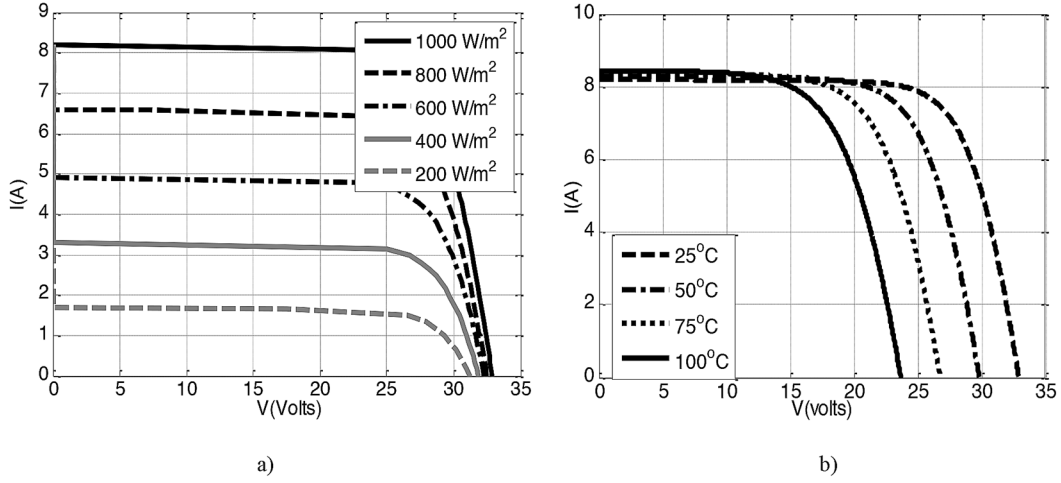
Fig. 2.   The I-V characteristics of Kyocera KC200GT from simulation with (a) varying irradiance at a cell temperature of $25°$C and; (b) varying cell temperature at 1000W/m^2.

TABLE I
PV PANEL PARAMETERS AT 1000 W/M^2 AND 25°C

Model	Kyocera KC200GT
P_{MPP}	200W
V_{MPP}	26.30V
I_{MPP}	7.61A
V_{OC}	32.90V
I_{SC}	8.21A

ideality factor usually chosen in the range $1 \le a \le 1.5$. Here a is taken as 1.

The photocurrent of the PV array depends linearly on the solar irradiance and the cell temperature, as shown by (2) [19].

$$I_{PV} = (I_{PV,n} + K_1 \Delta T) \frac{G}{G_n} \qquad (2)$$

where $I_{PV,n}$ is the photocurrent at the standard test condition (STC, 25°C and 1000 W/m^2); K_I is the short circuit current/ temperature coefficient; ΔT is the dtifference between the actual and nominal temperature in Kelvin; G is the irradiation on the device surface; and G_n is the nominal radiation, both in W/m^2.

$I_{PV,n}$ can be calculated based on (3)

$$I_{PV,n} = \frac{R_{sh} + R_s}{R_{sh}} I_{sc} \qquad (3)$$

Using these fundamental equations and parameters from the data sheet, the PV model is developed and verified with the panel datasheet. The I-V characteristics of KC200GT for different irradiance levels at the cell temperature of 25°C and varying cell temperature for a constant irradiance level of 1000 W/m^2 as obtained from the simulation are shown in Figs. 2(a) and (b), respectively. The similarities of the I-V curves for different conditions with the corresponding curves in the KC200GT panel datasheet prove the validity of the developed solar panel model. The parameters of the PV panel under study are shown in Table I.

The PV system under study for the proposed V-f and P-Q control has 125 strings with each string having 4 series connected panels. The Maximum Power Point (MPP) for a single panel of KC200GT at 1000 W/m^2 and 25°C (STC) is 200 W. Hence, the maximum power of the PV generator at STC is $125 \times 4 \times 200 = 100$ kW. The MPP varies according to the change in irradiance level and cell temperature.

IV. PV SYSTEM CONFIGURATION AND SYSTEM DESCRIPTION

A. PV System Configuration

Fig. 3 shows the PV system configuration for V-f and P-Q control with PV operating at MPP including the battery storage backup. It is a two-stage configuration where a DC-DC boost converter is used for MPPT control. The system also considers a battery back-up in case of emergencies while maintaining the voltage and frequency of the microgrid or while trying to supply the critical loads.

A battery is connected in parallel to the PV to inject or absorb active power through a bidirectional DC-DC converter. When the battery is absorbing power, the converter operates in the buck mode and when battery is injecting power to the grid, it operates in the boost mode. The operation mode is maintained through the control signal provided to the converter switches.

The PV system is connected to the grid through a coupling inductor L_c. The coupling inductor filters out the ripples in the PV output current. The connection point is called the point of common coupling (PCC) and the PCC voltage is denoted as $v_t(t)$. The rest of the system in Fig. 3 denotes the IEEE 13-bus distribution feeder which is simplified as a substation with the feeder equivalent impedance, $R + j\omega Ls$. The details of the IEEE-13 bus system will be described in the next section. The PV source is connected to the DC link of the inverter with a capacitor C_{dc}. The PV is the active power source, and the capacitor is the reactive power source of the PV system.

According to the instantaneous power definitions, for a balanced three-phase system, if $v_t(t)$ and $v_c(t)$ denote the instantaneous PCC voltage and the inverter output voltage (harmonics
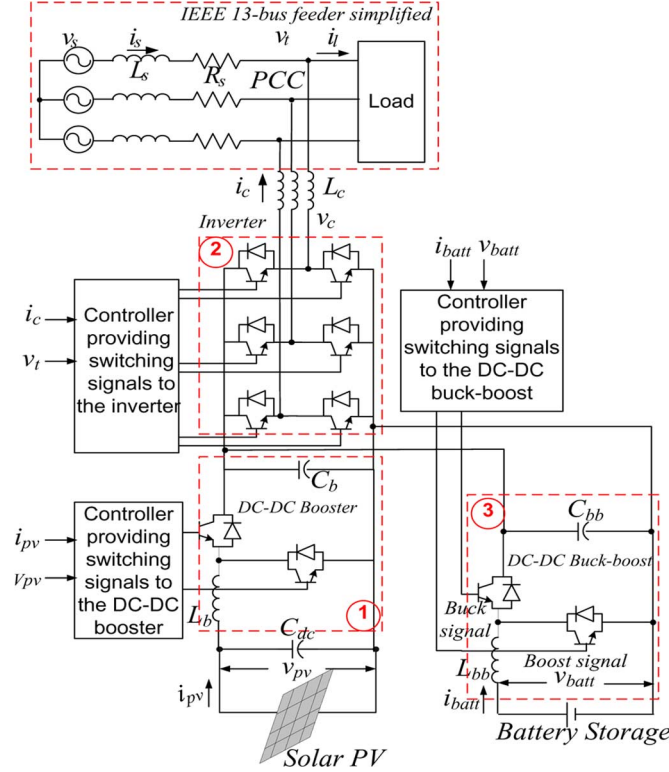
Fig. 3. System configuration of V-f control with solar PV generator operating at MPPT with a battery storage system.

neglected), respectively, then the average power of the PV denoted as $P(t)$, the apparent power $S(t)$ and the average reactive power $Q(t)$ of the PV are as given below [20]

$$P(t) = \frac{2}{T}\int_{t-\frac{T}{2}}^{t} v_t(\tau)i_c(\tau)d\tau = \frac{V_t(t)V_c(t)}{\omega L_c}\sin\alpha \qquad (4)$$

$$S(t) = V_t(t)I_c(t) = \frac{v_t(t)}{\omega L_c}\sqrt{V_t(t)^2 + V_c(t)^2 - 2V_t(t)V_c(t)\cos\alpha} \qquad (5)$$

$$Q(t) = \sqrt{S^2(t) - P^2(t)} = \frac{V_t(t)}{\omega L_c}(V_c(t)\cos\alpha - V_t(t)) \qquad (6)$$

Here, α is the phase angle of $v_c(t)$ relative to the PCC voltage. $P(t)$ and $Q(t)$ in (4) and (6) can be approximated by the first terms of the Taylor series if the angle α is small, as shown in (7) and (8):

$$P(t) \approx \frac{V_t(t)V_c(t)}{\omega L_c}\alpha \qquad (7)$$

$$Q(t) \approx \frac{V_t(t)}{\omega L_c}(V_t(t) - V_c(t)) \qquad (8)$$

B. Battery Modeling

In this paper, the battery model is taken from the MATLAB *SimPowerSystems* library with appropriate parameters which will be used for the proposed V-f and P-Q controls. The detailed description about the battery model is given in [21]. Due to the

intermittent and uncertain nature of solar power output and also the highly fluctuating load demands, deep cycle lead acid batteries are the most common type of battery storage in microgrid applications because the maximum capacity of the battery can be utilized. Hence, in this paper, a battery is modeled as a lead acid battery with appropriate choice of parameters for deep cycle application. It is assumed that the lead acid battery can be discharged up to SOC of 20% and can be charged up to SOC of 80%.

The battery model in [21] is an analytical model with two equations representing the battery discharge and charge models. The battery discharge and charge model for a lead acid battery is given by (9) and (10), respectively

$$V_{\text{Batt}} = V_0 - R \cdot i - K\frac{Q}{Q - \text{it}}(\text{it} + t^*) + \text{Exp}(t) \qquad (9)$$

$$V_{\text{Batt}} = V_0 - R \cdot i - \left[K\frac{Q}{\text{it} - 0.1Q}\right]i^* - \left[K\frac{Q}{Q - \text{it}}\right]\cdot\text{it} + \text{Exp}(t) \qquad (10)$$

where V_{batt} is the battery voltage (V), V_o is the battery constant voltage (V), K is polarisation constant (V/Ah) or polarisation resistance (Ω), Q is battery capacity (Ah), it $= \int idt =$ actual battery charge (Ah), A is exponential zone amplitude (V), B is exponential zone time constant inverse (Ah^{-1}), R is the internal resistance(Ω), i is battery current (A), and i^* is filtered current (A).

In this model, the term for polarisation voltage and polarisation resistance is considered to model the Open Circuit Voltage (OCV) of the battery more accurately. The term inside the first square bracket in (10) represents the polarisation resistance and the second square bracket represents the polarisation voltage.

The size of the battery is selected to provide a maximum backup power to compensate for the PV generation in the case of a very small or no irradiance level. In this work, the MPP of PV generator at STC is 100 kW. Hence, the battery is chosen to provide this amount of power for a maximum of 1 hour with an energy content of 100 kWh. The battery backup is considered for short duration applications like frequency control and supplying power to critical loads in the event of emergency situations. One hour of battery backup is considered to be enough for other backup generators to take over the controls in the microgrid emergency situations.

C. Description of IEEE 13-Bus Distribution Feeder

The diagram of the IEEE 13-bus distribution test system is shown in Fig. 4. It consists of a substation, 13 buses or nodes, 11 line sections, and 8 loads. The loads comprise of a combination of constant impedance, constant current, and constant power (ZIP) loads but most of them are constant power loads. The substation is at 115 kV and it is stepped down to 4.16 kV by a distribution transformer (T1). There is one more transformer (T2) which steps down 4.16 kV to 480 V.

In the grid connected mode, the substation located at Bus 650 at 115 kV level is considered as a source. In an islanded microgrid case, a diesel generator connected at the same bus supplies the microgrid with a fixed amount of active power as referenced by the central controller (CC) of the microgrid.
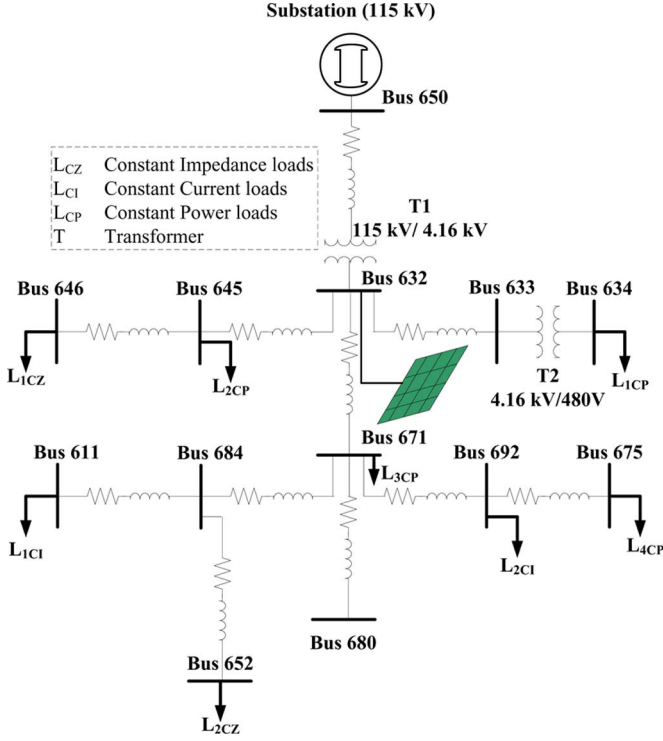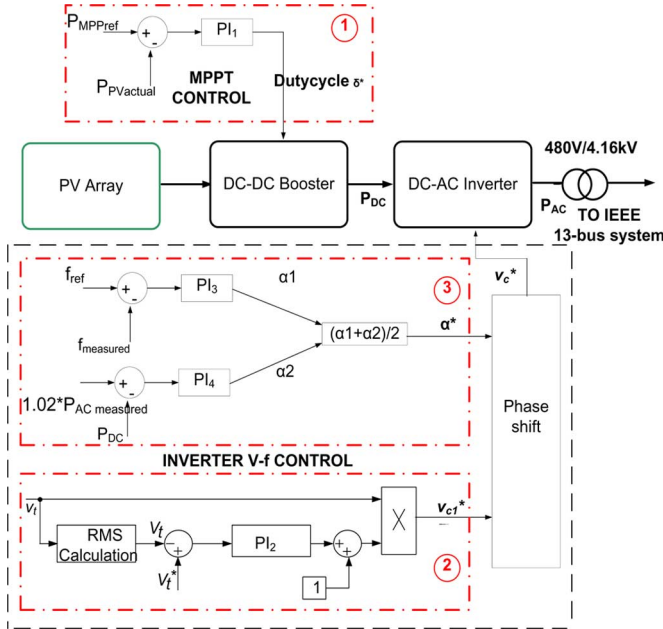
Fig. 4. IEEE-13 bus distribution feeder.

Fig. 5. Integrated Solar PV MPPT and V-f control diagram.

V. MPPT AND BATTERY INTEGRATED V-F AND P-Q CONTROL METHODS

A. MPPT and Battery Integrated V-f Control Method

The MPPT and battery integrated V-f control diagrams are shown in Figs. 5 and 6, respectively. The control comprises of one loop for MPPT control, two different loops for V-f control at the inverter side and another loop for battery power management.
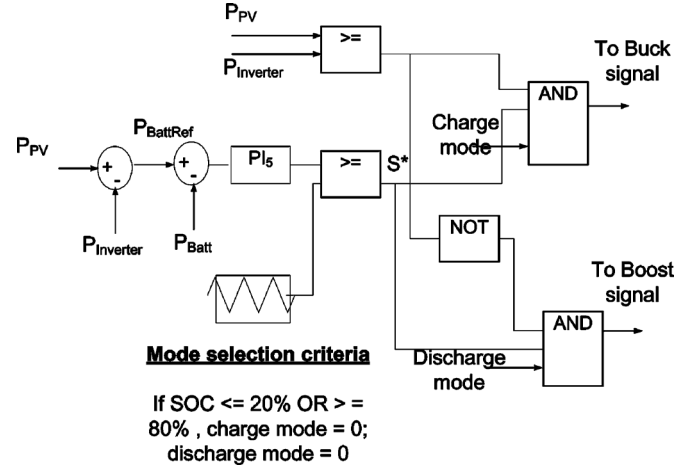

Fig. 6. Battery power control diagram.

The loop 1 in Fig. 5 is a MPPT control at the PV array side which uses the reference MPP, P_{MPPref} from the look up table of irradiance versus MPP. Then, it compares the actual PV power output, P_{PV} with this reference and feeds this error to a PI controller, PI_1 which outputs the duty cycle δ^* for the DC-DC booster so that the array always operates at the referenced point. The equation for this control loop is given by (11). Here, K_{p1} and K_{i1} are the controller proportional and integral gains respectively

$$\delta^* = K_{p1} * (P_{\mathrm{MPPref}} - P_{\mathrm{PV}}) + K_{i1} * \int_0^t (P_{\mathrm{MPPref}} - P_{\mathrm{PV}})dt.$$

(11)

Another feedback PI controller PI_2 is used for voltage control at AC side. As shown in the control diagram in Fig. 5 (loop 2), the PCC voltage is measured and the rms value of $v_t(t)$ is calculated. Then, the rms value $V_t(t)$ is compared to a voltage reference $V_t^*(t)$ which could be a voltage specified by the utility, and the error is fed to a PI controller. The inverter output voltage $v_c(t)^*$ is controlled so that it is in phase with the PCC voltage, and the magnitude of the inverter output voltage is controlled so that the PCC voltage is regulated at a given level $V_t^*(t)$. The control scheme can be specifically expressed as (12).

$$v_{c1}^*(t) = v_t(t) \left[1 + K_{P2}(V_t^*(t) - V_t(t)) \right.$$
$$\left. + K_{I2} \int_0^t ((V_t^*(t) - V_t(t))dt) \right] \quad (12)$$

where K_{P2} and K_{I2} are the controller gains for this loop.

In (12), 1 has been added to the right-hand side such that when there is no injection from the PV generator, the PV output voltage is exactly the same as the terminal voltage.

The frequency control is carried out by controlling the active power output at the inverter side as shown in the outermost loop 3. The referenced microgrid frequency of 60 Hz is compared with the measured value and this error is fed to the PI controller PI_3 that provides the phase shift contribution α_1^* which shifts the voltage waveform in timescale such that the active power

injected will be enough to maintain the frequency at 60 Hz nominal value. The equation for this control is given by (13)

$$\alpha_1^* = K_{P3}(f_{\text{ref}} - f_{\text{measured}}) + K_{I3} \int_0^t (f_{\text{ref}} - f_{\text{measured}})dt \tag{13}$$

There is another controller PI_4 used in the same loop 3. This controller maintains active power balance between the AC and DC sides of the inverter. The reference signal for PI_4 is obtained from the dynamically changing active power injection from the inverter at the AC side as determined by the output of PI_3. The measured AC side active power, $P_{\text{ACmeasured}}$ is multiplied by a factor of 1.02 considering the efficiency of inverter as 98% such that the DC side active power is 102% of the AC side active power. The DC side active power is compared with this value of AC side power and the error is fed to PI_4 to obtain the phase shift contribution from this loop as α_2^*. The equation for this control is given by (14)

$$\alpha_2^* = K_{P4}(1.02 * P_{\text{AC}} - P_{\text{DC}})$$
$$+ K_{I4} \int_0^t (1.02 * P_{\text{AC}} - P_{\text{DC}})dt. \tag{14}$$

The phase shift contributions from DC and AC sides, α_1^* and α_2^* are then averaged as given by (15) to obtain the final phase shift, α^* of the voltage waveform, v_{c1*} which, then, generates the voltage reference signal v_{c*} for the inverter PWM

$$\alpha^* = (\alpha_1^* + \alpha_2^*)/2. \tag{15}$$

Here, the reason behind considering phase shift contributions from both DC and AC side active power is to control the DC side voltage and achieve the desired value. By making α_1^* and α_2^* close in range through the controller gains, it can be assured that the active power at the DC and AC sides is balanced. This, coupled with the voltage control loop, assures that the DC side voltage is maintained at the value desired by the AC side voltage.

The controls shown in the diagram of Fig. 5 and described above are also integrated with the battery power control shown in Fig. 6. The battery is incorporated in the PV system configuration in order to supply or absorb active power and support the frequency control objective with the PV generator. If there is abundant solar power and the active power required for frequency control is less than PV MPP, then the battery will be charged. If there is not enough solar power available and if the active power required for frequency control is more than PV MPP, then the battery will supply the deficit power in order to maintain the microgrid frequency at 60 Hz. Hence, the control method for the battery charge/discharge that depends on this requirement is developed as shown in Fig. 6. It also shows the selection of charge and discharge modes which handle the battery SOC constraint and will be described later in the Part B of this section.

In Fig. 6, the reference power to the battery, P_{Battref} is generated dynamically by subtracting the inverter active power injection, P_{inverter} from the power generated by PV, P_{PV}. The controller comprised of a PI controller, PI_5 which receives the error signal obtained after subtracting the actual battery power, P_{batt} from the battery reference, P_{Battref}. The signal obtained

from PI_5 is then compared with a triangular waveform of unity magnitude to generate the signal, S^*. This is similar to common Pulse Width Modulation (PWM) in inverter controls. K_{p5} and K_{I5} are the proportional and integral gains respectively. The equation for this control is given by (16)

$$S^* = K_{P5}(P_{\text{Battref}} - P_{\text{Batt}}) + K_{15} \int_0^t (P_{\text{Battref}} - P_{\text{Batt}})dt. \tag{16}$$

One more step is considered to differentiate the charging and discharging mode of the battery. This is undertaken by comparing P_{PV} with P_{inverter}. If $P_{\text{PV}} >= P_{\text{inverter}}$, the battery is in charging mode, hence, the signal obtained from the PWM, S^* and the result of this comparison is passed through a logical AND to generate a switching signal which activates the Buck mode of the DC-DC converter. If the condition $P_{\text{PV}} >= P_{\text{inverter}}$ is false, (i.e., $P_{\text{PV}} < P_{\text{inverter}}$), the opposite of this signal and S^* is passed through a logical AND to generate a switching signal which activates the Boost mode of the DC-DC converter. Hence, with this control logic, the converter is capable of operating in both directions and therefore, effectively charging and discharging the battery whenever required. This will be verified through the results presented in Section VI of this paper.

B. Modification of V-F Control With Battery SOC Constraint

When there is abundant solar irradiance available and the active power required for the microgrid frequency control is less than active power produced by the PV generator at MPP i.e., $P_{\text{fcontrol}} < P_{\text{PVMPP}}$ and at the same time the battery SOC is 80%, then, the battery cannot be charged beyond this upper limit of SOC. In such case, decreasing the output power of PV generator would lead to underutilization of the solar resource. Hence, a global control mechanism is required in a microgrid which can transition the PV control from frequency control mode to constant power mode with power to be generated at P_{PVMPP}. Meanwhile, there should be a mechanism to allow any other generator of the microgrid to handle the frequency control problem. In the microgrid system under consideration, there is a diesel generator which can decrease its generation in order to match the PV generation increase. Hence, the power balance of the system will be maintained in order to control the microgrid frequency.

Similarly, when the irradiance is low such that the maximum power from PV generator is not enough to maintain the microgrid frequency i.e., $P_{\text{fcontrol}} > P_{\text{PVMPP}}$ and at the same time, the battery SOC is 20%, then the battery will not be able to back up the PV generator. In such case, the frequency control function needs to be transferred to other available generator if possible, in this case, a diesel generator. Again, a global control mechanism becomes an absolute necessity for allowing the transition of PV generator control from frequency control mode to constant MPP mode and the diesel generator control from constant active power mode to frequency control mode such that the frequency stability of the microgrid can be achieved.

Figs. 6, 7, and 8 show the modifications of controls at different stages in the microgrid in order to handle the above situations. Fig. 7 shows the transition of the diesel generator control from constant active power control to frequency control. Instead of considering the error between the reference electrical power
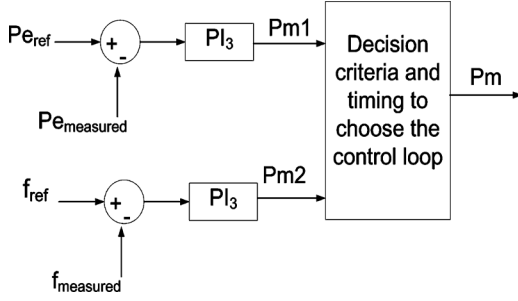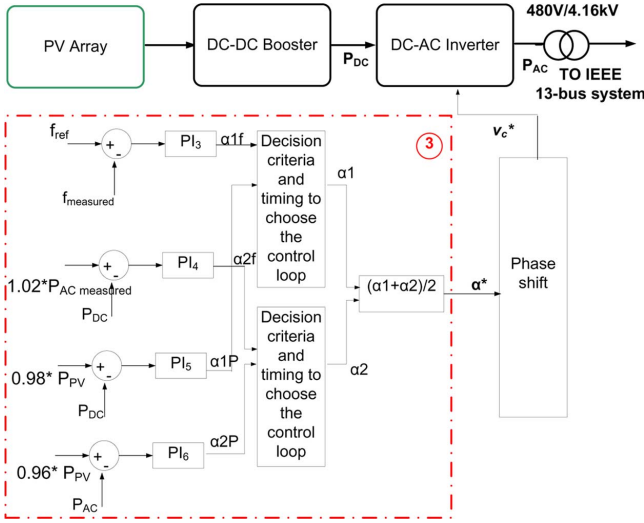
Fig. 7. Diesel generator control transition.

Fig. 8. Modification of PV inverter frequency control loop.

Fig. 9. Integrated Solar PV MPPT and PQ control diagram.

and the measured electrical power to generate the mechanical power reference, the frequency error is considered in the controls. Fig. 8 shows the modification in frequency control loop of the PV inverter which includes the transition to another constant active power control loop. During the simulation process, the transition time is heuristically selected as 8 sec so that the smoothness in the transfer of controls can be observed.

The slight modification required in the battery control for taking care of the battery SOC is also shown in Fig. 6. It includes incorporation of a signal for selecting the charge or discharge mode of the battery. When the SOC >80% or SOC <20%, then, both the charge and discharge mode are given the value of 0 such that the output is always zero for these two cases. In other cases, the charge mode would take a value of 1 and the discharge mode would take a value of 0 if the battery is charging, and vice versa if the battery is discharging.

With these modifications in the existing control structure, the IEEE 13-bus system acting as a microgrid can handle the problem of under frequency and voltage during islanding through the proper coordination of the participating generators even without the battery. This can be observed from the results to be presented later in Section VI-B.

C. MPPT and Battery Integrated P-Q Control Method

This sub-section presents the proposed coordinated active and nonactive/reactive (P-Q) power control integrated with PV MPPT and battery controls. Either in grid connected or islanded mode, the microresources may be required to supply critical loads like hospitals, industries, etc. The proposed
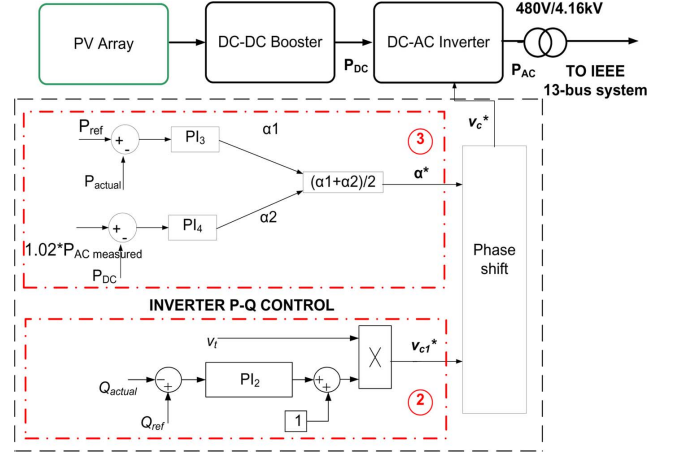
control strategy is applicable particularly for such cases. The MPPT control part for generating the duty cycle of a proper control for the DC-DC boost converter is the same as described in Section V-A above and hence, will not be explained here. Thus, Fig. 9 shows the P-Q control blocks only, leaving behind the MPPT control block which is also present in the entire integrated control system. The P-Q control initially proposed in [22] and implemented in a larger system in [23] is converted to a more robust control with the integration of MPPT control and battery storage control in the present work.

The inverter side P-Q control is slightly modified version of inverter V-f control. It is entirely based on the relationship of active and reactive power at PCC with inverter output phase and voltage magnitude as given by the (7) and (8), respectively. In Fig. 9 (loop 2), the measured reactive power injection at PCC is compared with the referenced reactive load and this error signal is passed to the PI controller, PI_2. Then, the term obtained is multiplied by the terminal voltage v_t to obtain the reference voltage v_{c1}^* which is in phase with v_t. The control loop 3 in Fig. 9 handles active power control through the controller, PI_3 to generate the phase shift contribution α_1^* and at the same time insure the active power balance between AC and DC sides through the controller, PI_4. This is already explained in detail in Section V-A for V-f control. Thus, the equations for P-Q control are given by (17)–(20)

$$v_{c1}^* = (K_{P2}(Q_{\text{ref}} - Q_{\text{actual}})$$
$$+ K_{I2} \int_0^t (Q_{\text{ref}} - Q_{\text{actual}})dt + 1)v_t \tag{17}$$

$$\alpha_1^* = K_{P3}(P_{\text{ref}} - P_{\text{actual}})$$
$$+ K_{I3} \int_0^t (P_{\text{ref}} - P_{\text{actual}})dt \tag{18}$$

$$\alpha_2^* = K_{P4}(1.02 * P_{\text{ACmeasured}} - P_{\text{DC}})$$
$$+ K_{14} \int_0^t (1.02 * P_{\text{ACmeasured}} - P_{\text{DC}})dt \tag{19}$$

$$\alpha^* = (\alpha_1^* + \alpha_2^*)/2 \tag{20}$$

Equation (17) represents the reactive power control loop, (18) represents the active power control loop, and (19) ensures the active power balance between the DC and AC sides of the inverter. Equation (20) averages the phase shift contribution obtained from the active power control at the AC and DC sides

TABLE II
CONTROLLER GAIN PARAMETERS FOR V-F CONTROL (CASE 1)

MPPT Control Loop	K_{p1}	6×10^{-8}
	K_{i1}	6×10^{-6}
Voltage Control Loop	K_{p2}	0.0004
	K_{i2}	0.005
Frequency Control Loop	K_{p3}	9.9×10^{-4}
	K_{i3}	5×10^{-3}
P_{DC} Control Loop	K_{p4}	0.8×10^{-9}
	K_{i4}	0.8×10^{-8}
Battery Control Loop	K_{p5}	1.5×10^{-8}
	K_{i5}	1.5×10^{-7}

such that the active power control at AC side and power balance objectives are taken into account.

The battery control integrated into the P-Q control is the same as the one described in the Section V-A.

VI. SIMULATION RESULTS AND DISCUSSIONS

This section presents the simulation results obtained with applications of the proposed control methods to the IEEE 13-bus distribution feeder presented in Section IV-C. First, the results obtained from the coordinated V-f control are presented which is followed by the results from the coordinated P-Q control. In grid connected mode, the distribution feeder is considered to be supplied by a central generator with a substation at Bus 650 at 115 kV level and a PV generator at Bus 632. Hence, in an islanded case, the distribution feeder is supplied by a diesel generator and a PV connected at Buses 650 and 632, respectively.

A. Test of V-F Control in Microgrid Mode

For the demonstration of the V-f control algorithm, two different irradiance cases are considered: Case 1 with Irradiance = 1000 W/m² and Case 2 with Irradiance = 750 W/m². The PI controller gain parameters for Case 1 are given in Table II. The controller gains should be adjusted slightly for the change in irradiance.

While moving from the grid connected to microgrid mode, the diesel generator is controlled to generate a fixed amount of active power according to the command from the central controller. The diesel generator produces a fixed amount of 1.25 MW throughout the simulation period as shown in Fig. 10(a). It also shows the reactive power generated from the diesel generator.

In the islanded mode, the active power generated by the diesel generator is not enough to fulfill the power demand of the microgrid. Fig. 10(b) shows the microgrid frequency which initially dips to a value of 57.8 Hz due to the load-generation imbalance. The frequency control from the PV generator starts at 2.2 sec which quickly regulates the frequency back to 60 Hz in 2 sec. Fig. 10(c) shows the plot of the PCC voltage in p.u. It can be observed that voltage is also quickly regulated at 1 p.u. after the control is started.

Fig. 10(d) shows the active and reactive power injection from the PV inverter which regulates the frequency and voltage of the microgrid. The active power injection from the inverter, which is required to maintain the frequency at 60 Hz in both cases, is around 80 kW. However, there is a difference in the share
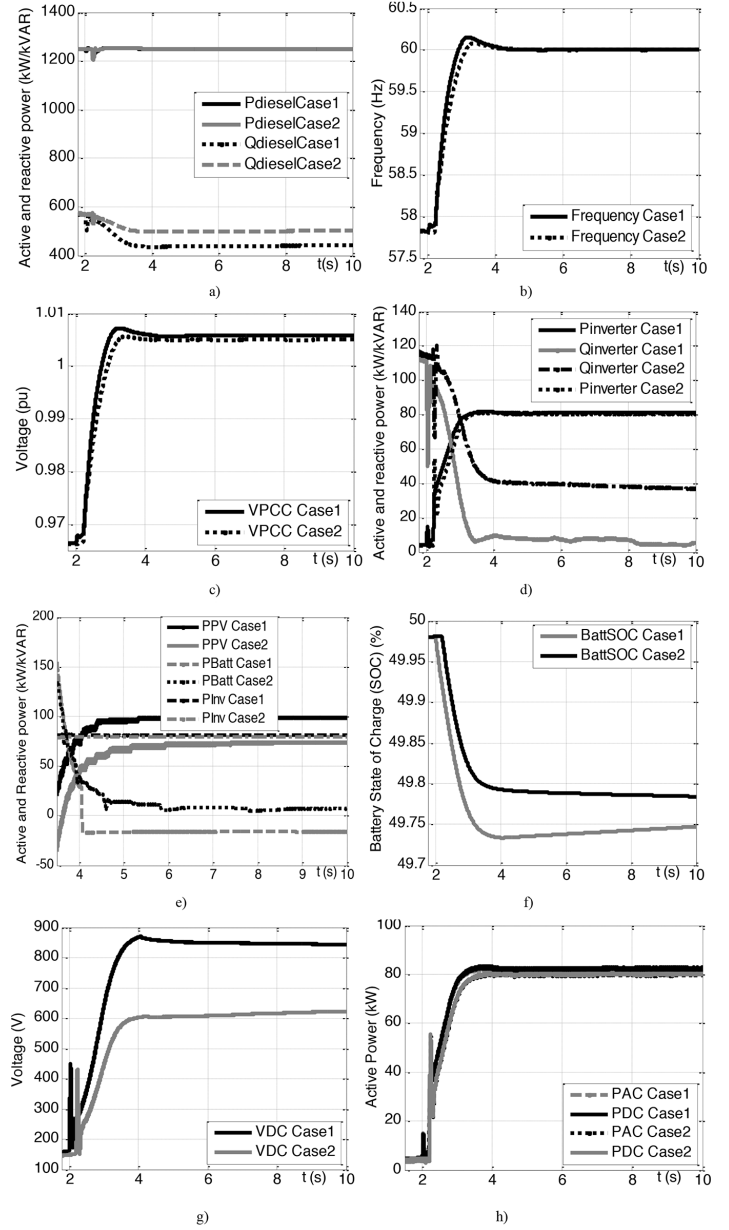

Fig. 10. Results of coordinated V-f control with solar PV including MPPT control and battery control.

of the PV generator and the battery energy storage while providing the required 80 kW to the microgrid. This is evident from Fig. 10(e) which shows the active power from the PV, the battery, and the inverter, respectively, for both cases. In Case 1, solar irradiance is abundant at 1000 W/m² and hence, the PV generates the maximum power of 100 kW which is more than is required to maintain the microgrid frequency. The surplus 20 kW is used to charge the battery. The negative sign in battery power means that it is a charging phase, i.e., the battery absorbs power. In Case 2, PV generates only around 75 kW at MPP due to decreased irradiance. This is not sufficient to maintain the microgrid frequency at 60 Hz. Hence, the deficit power of around 5 kW is supplied by the battery as shown by the 4th (PBatt Case 2) curve in Fig. 10(e). Here, the positive sign of battery power means that it injects active power into the microgrid.
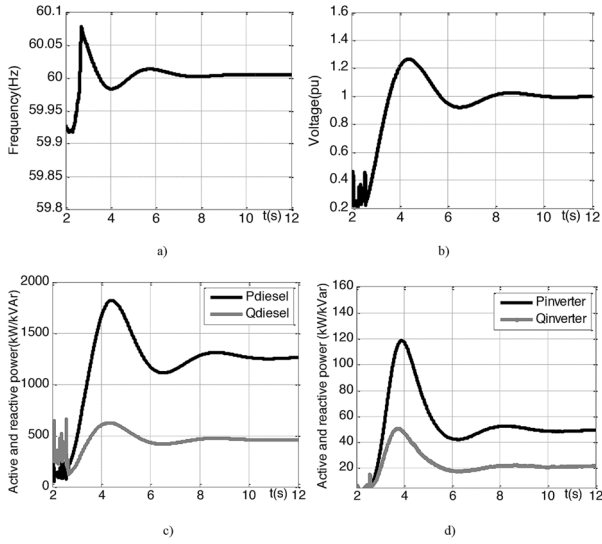
Fig. 11.   Results for V-f control of microgrid with diesel generator.

Fig. 12.   Results of V-f control showing grid to microgrid transition.

Fig. 10(f) shows the state of charge (SOC) of the lead acid battery considered for this study. The gray curve represents the SOC for Case 1 which shows that it gradually increases as the excess power is fed to charge the battery. The decreasing black curve for Case 2 in Fig. 10(f) shows that the power is being extracted from the battery.

Fig. 10(g) shows the DC voltage for both cases. It can be seen that the voltages are stably maintained at around 850 V and 550 V respectively for the two cases. Fig. 10(h) shows the active power at the DC and AC sides of the inverter for both cases. It is clear that DC active power is slightly higher than the AC side three phase average power. This accounts to some percentage (taken as 2% in the present work) of power losses between the DC and AC sides but the overall active power is balanced through controls. This power balance coupled with the AC side voltage control maintains the DC side voltage to a stable value which is the uniqueness of the proposed coordinated MPPT and inverter control.

Fig. 11(a) through (d) show the results obtained when the diesel generator is involved in the voltage and frequency regulation of the microgrid and the solar PV is controlled to dispatch constant active and reactive power. The V-f control of the diesel generator also starts at 2.2 sec just as in the case of the V-f control with PV generator and battery. Fig. 11(a) shows the frequency of the microgrid which shoots up in the beginning and then, gradually decreases and stays at 60 Hz in around 8 sec. It is clear from this figure that the diesel generator takes much longer time to recover the frequency than the PV and battery combination as discussed above. Fig. 11(b) shows the voltage plot of the microgrid. It is also clear that it takes around 10 sec for the voltage to settle down to 1 pu.

Fig. 11(c) shows the power generated from the diesel generator and Fig. 11(d) shows the active and reactive power injection from the PV inverter which is operated at constant PQ mode. It takes about 10 sec for all the injections to stably reach the desired values. It is worth noting that the injection from the PV inverter is also affected by the oscillations in diesel generator output for the first few seconds before reaching the steady state. Hence, it is clearly verified that solar PV and battery without in-
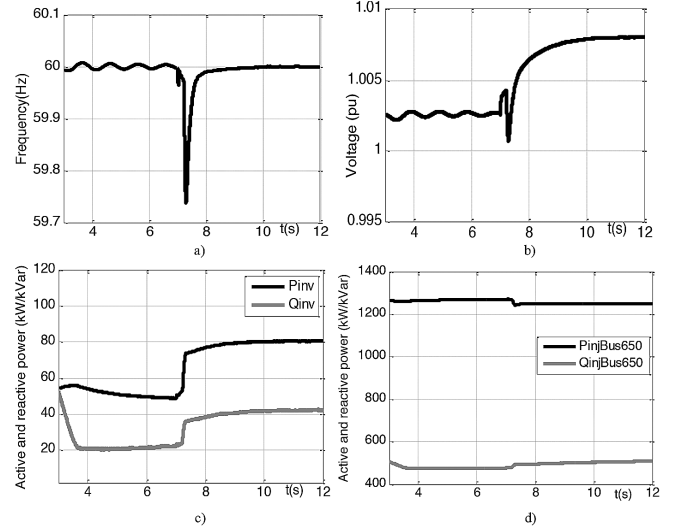
ertia can perform the V-f control for microgrid much faster than the diesel generator with inertial effect.

B. Test of V-F Control Showing Transition From Grid Connected to Islanded Microgrid Mode

A separate case study is carried out to show the dynamic characteristics of the proposed V-f and P-Q control algorithms while transitioning from the grid connected to microgrid structure. For this study, Case 1 of Section VI-A is considered in which the irradiance is at 1000 W/m^2. The bus 650 is connected to the substation in the grid connected mode and in the islanded case, the tie switch is opened at t = 7 sec. The microgrid is then fed only by the diesel generator located at the same bus 650, and the PV generator and battery at bus 632. Fig. 12(a) shows the frequency of the system and voltage at PCC both in grid connected and islanded cases. It can be observed that the islanded microgrid frequency is quickly revived back to 60 Hz in less than 1.5 sec after the islanding occurs at 7 sec. A similar response can be observed in the voltage profile at PCC as shown in Fig. 12(b). This is due to the faster control characteristics of PV and battery integrated system involved in V-f control in islanded case.

Fig. 12(c) shows the active and reactive power injection from the PV inverter. The PV is controlled to a constant active power of around 50 kW and constant reactive power of around 20 kVar in a grid connected mode. Both active and reactive power injections from PV increase as the microgrid transitions to the islanded case in which PV is responsible for maintaining the microgrid frequency and voltage at PCC. Fig. 12(d) shows the power injection at Bus 650 of the IEEE 13-bus system. The injection is from the substation in the grid connected mode. In contrast, in islanded mode, the injection comes from the diesel generator which is maintained at a constant value of 1.25 MW. The results presented here clearly show the effectiveness of the V-f and P-Q control algorithms even when the microgrid transitions from the grid connected to the islanded mode.

C. Test of V-F Control With Battery SOC Constraint

In the present work, SOC of the lead acid battery used in the microgrid is considered to be in the range of 20%–80%.
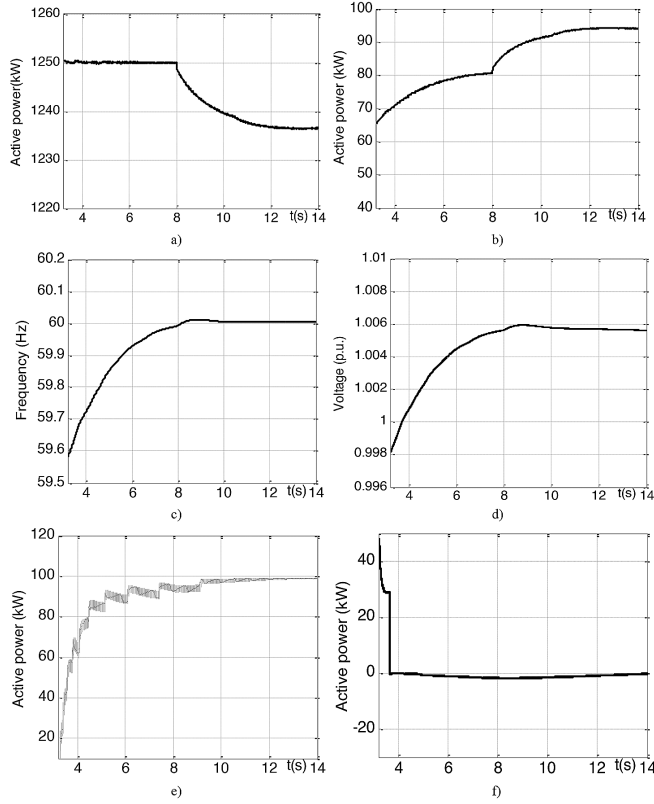
Fig. 13. Results of V-f control with MPPT and battery considering battery SOC upper constraint (80% charged: Case 1).

Fig. 14. Results of V-f control with MPPT and battery considering battery SOC upper constraint (20% charged: Case 2).

In the above discussions, the proposed V-f control algorithm is verified by considering the case in which there is enough room to charge or discharge the battery in the microgrid. But, there could be a situation when the battery SOC is on the verge of these upper and lower boundaries.

Fig. 13((a) through (f)) show the results obtained from this transition of controls at the PV inverter and the diesel generator. Fig. 13(a) and (b) show the active power from the diesel generator and the PV inverter. It can be observed that the PV generator which performs frequency regulation of microgrid before $t = 8$ sec, quickly transitions to generate at MPP with the irradiance level of 1000 W/m^2, whereas the diesel generator active power control, which was otherwise maintained at the active power output at 1250 kW, quickly transitions to the frequency control mode. Hence, the diesel generator decreases its active power output to around 1237 kW to cope with the increase in generation of the PV generator. Figs. 13(c) and (d) show the microgrid frequency and voltage at PCC which are maintained at 60 Hz and around 1 p.u., respectively, as a result of the proposed controls. The slow response speed is observed while achieving the referenced values of voltage and frequency due to the involvement of diesel generator in frequency control. Figs. 13(e) and (f) show the active power from the PV generator and the battery, respectively. The PV generates at the maximum power of around 100 kW and the battery power is almost zero showing that it does not absorb any power. This means that it is not charged even though the PV generation is higher than what is required for frequency control as the SOC of the battery is at the maximum for this case.
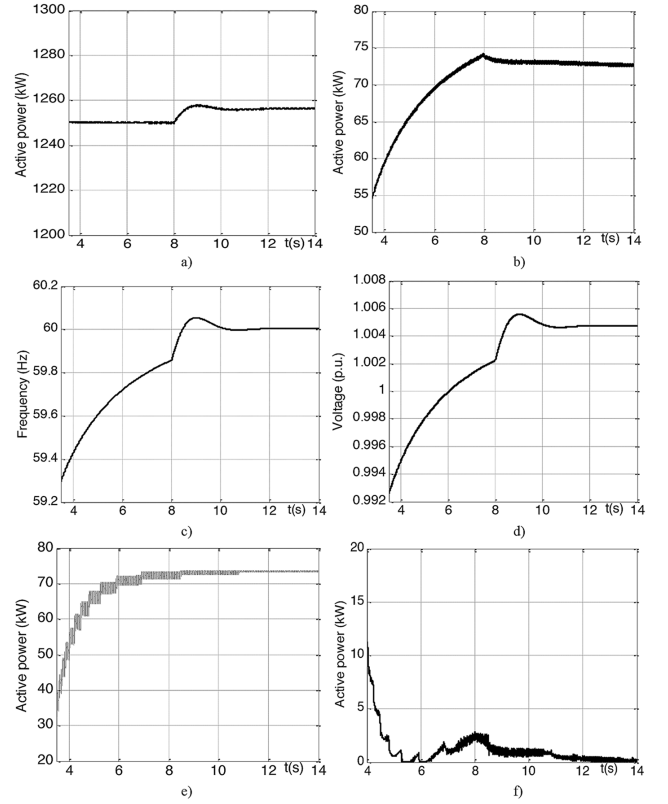
Similarly, an equally opposite scenario is possible. Assume the solar irradiance is low such that the maximum power generated by the PV generator is not enough to provide the frequency control, i.e., $P_{fcontrol} > PV_{MPP}$. In such case, if the battery SOC is 20%, the battery cannot provide extra active power required for frequency control. In this case, the PV generator control should transition from frequency control to constant active power at MPP control, and the frequency control function should be taken over by the participating diesel unit which otherwise produces a constant active power of 1250 kW. In this case, P_{PVMPP} is approximately 75 kW which is less than 80 kW required for frequency control. The deficit active power should be provided by the diesel generator in order to maintain the system frequency at 60 Hz. Because of this transition of control from constant active power to frequency control, the diesel generator's active power increases to 1255 kW, therefore, fulfilling the requirement for frequency control. The PV generator, on the other hand, is maintained at a constant power of around 72 kW equal to $0.96 \times P_{PVMPP}$. The plots of active power generation from the diesel generator and the injection from the PV inverter are shown in Figs. 14(a) and (b), respectively.

Figs. 14(c) and (d) show the microgrid frequency and voltage at PCC, respectively. It is clear that the PV generator was initially trying to control the frequency but could reach only a value below 60 Hz due to low active power injection from the inverter. However, as the frequency control transfers from the PV generator to the diesel generator at 8 sec, it quickly returns to 60 Hz in around 2 sec. A similar nature of results can be observed for the voltage at PCC which is stably maintained at 1.005 p.u. after

TABLE III
CONTROLLER GAIN PARAMETERS FOR P-Q CONTROL (CASE 3)

MPPT Control Loop	K_{p1}	6×10^{-8}
	K_{i1}	6×10^{-6}
Voltage Control Loop	K_{p2}	5×10^{-8}
	K_{i2}	5×10^{-7}
P_{AC} Control Loop	K_{p3}	2.5×10^{-9}
	K_{i3}	2.5×10^{-8}
P_{DC} Control Loop	K_{p4}	2.5×10^{-9}
	K_{i4}	2.5×10^{-8}
Battery Control Loop	K_{p5}	0.02×10^{-8}
	K_{i5}	0.02×10^{-7}

the transition of controls. Figs. 14(e) and (f) show active power output of the PV generator and the battery. The PV generates the MPP power of 75 kW and the battery power is close to zero showing that the battery is not able to inject any power in this case as SOC is at its minimum limit.

D. Test of P-Q Control

The results of P-Q control with integrated MPPT and battery control is presented in Fig. 15 (a)–(f). Like V-f control, two different cases, namely Case 3 and Case 4, are considered for simulation validation of this control as well. Cases 3 and 4 are similar to Cases 1 and 2 with slight differences which are elaborated in the following paragraph. The controller gain parameters for Case 3 are given in Table III. The parameters need to be readjusted slightly for Case 4.

Here, in Case 3, the critical active power load of a microgrid is less than the maximum available PV power (i.e., $P_{ref} <= P_{PV}$), and in Case 4, $P_{ref} > P_{PV}$. Hence, the disturbance for this part is the load changes which are very common in real operation. Moreover, since coordinated P-Q control method is to be validated, the load change is the most representative scenario to study the effectiveness of the proposed control. Hence, the solar irradiance is considered constant at 1000 W/m^2 for both cases.

Fig. 15(a) shows the active and reactive power from the diesel generator. The diesel genset produces a constant active power of 1250 kW throughout the simulation period for both cases with a slight change in reactive power between the two cases. Fig. 15(b) shows the reference and actual active and reactive power of the PV inverter. The reference values of active power represent the critical loads of the microgrid as previously mentioned. The references of the active power for Cases 3 and 4 are 50 kW and 120 kW, respectively. Similarly, the references of the reactive power for Cases 3 and 4 are 20 kVAR and 70 kVAR, respectively. The references are chosen to demonstrate both charging and discharging processes of the backup battery energy storage system. It can be observed from Fig. 15(b) that the proposed coordinated controls are capable of serving the critical loads in as little as 2 seconds.

Fig. 15(c) shows the plot of active power from the PV generator, the inverter injection, and the active power to and from the battery. In both cases, the power from PV is maintained constant at the MPP power of 100 kW through MPPT controls as shown by the overlapping black and gray solid curves. The active power injection from the inverter is maintained at the reference values
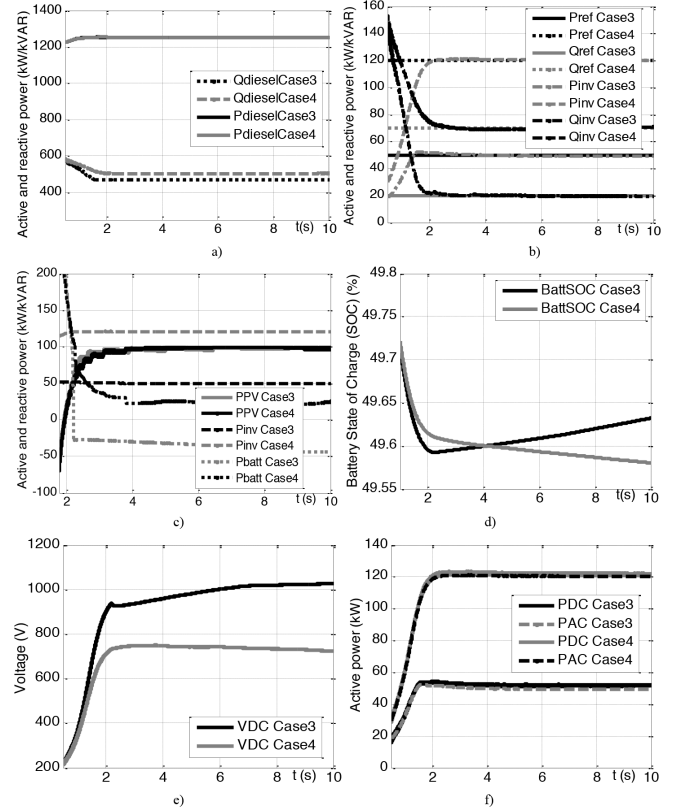

Fig. 15. Results of coordinated P-Q control with solar PV including MPPT control and battery control.

of 50 kW and 120 kW in Cases 3 and 4, respectively. These reference values are demanded by the critical loads. The generation from PV in Case 3 is more than the critical load by 50 kW. Thus, this surplus power is sent to charge the lead acid battery which is shown by the 5th (Pbatt Case3) curve in Fig. 15(c). The negative sign of power from the battery shows that it is being charged.

For Case 4, the critical load is greater than the PV generation at MPP and the deficit power of 20 kW is supplied by the battery as shown by the 6th (Pbatt Case4) curve in Fig. 15(c). As explained earlier, the positive sign of power from the battery shows that it is being discharged. Therefore, for Case 3, the power injection from the inverter comes only from the solar PV generator. However, in Case 4, the injection comes from PV and battery.

Fig. 15(d) shows the SOC of the battery. It is clear that the SOC increases in Case 3 and decreases in Case 4 as expected because of the respective charging and discharging scenarios. It also validates the effectiveness of the battery control algorithm adopted in controlling the bidirectional power flow to and from the battery.

Fig. 15(e) shows the DC side voltage at the inverter input. It is stably maintained at around 1012 V and 740 V for Cases 3 and 4, respectively. It validates the indirect control of the DC side voltage through the power balance between AC and DC sides of the inverter. Similarly, Fig. 15(f) shows the active power measured at the DC and AC sides of the inverter. Clearly, the DC side active power is slightly greater than the AC side power which means that the control algorithm also takes care of the efficiency of the inverter in the model. Hence, the effectiveness of the proposed coordinated P-Q control algorithm in microgrids is clearly demonstrated from the presented results.

VII. Conclusion

The contribution of this paper can be summarized as follows:

- This paper proposes and presents coordinated strategies of V-f control and P-Q control, respectively, for microgrids with PV generator and battery storage.
- In the control strategies, the PV generator is operated at MPP, and the battery storage acts as a buffer in order to inject and absorb deficit or surplus power by using the charge/discharge cycle of the battery. The paper contributes in demonstrating the control strategies with effective coordination between inverter V-f (or P-Q) control, MPPT control, and energy storage control.
- The proposed control strategy also provides a smooth transition of PV side PQ control in grid connected mode to V-f control in islanded mode. This is the most essential feature required in the modern microgrid controllers.
- The proposed control algorithms are also capable of handling the battery SOC constraint. An effective seamless transformation of controls from V-f to constant active power and voltage control at the PV side and from constant active power control to frequency control at the diesel generator is validated with satisfactory results. This feature helps the controller to adapt to the changing irradiance levels while considering the battery availability.
- The proposed V-f control method shows a very satisfactory performance in reviving highly reduced voltage and frequency back to the nominal values in a matter of only 2 seconds. It is much faster than the diesel generator control which takes around 10 seconds to settle down. Hence, PV and battery installations might be applied effectively in restoring the microgrid frequency and the voltage at PCC after disturbances.
- Similarly, the proposed integrated and coordinated P-Q control algorithm can be effectively used in supplying some critical loads of a microgrid with solar PV and battery.

In the present methods, the control parameters are dependent upon the PV, battery, and external grid conditions and must be re-tuned with the changing conditions. This can be overcome by using an adaptive method to obtain these parameters dynamically based on the system conditions. The adaptive control methods could be a very useful and promising future direction of this work.

References

[1] R. H. Lasseter, "MicroGrids," in *Proc. IEEE Power Engineering Society Winter Meeting*, 2002, vol. 1, pp. 305–308.

[2] S. Chowdhury, S. P. Chowdhury, and P. Crossley, "Microgrids and Active Distribution Networks," 2009, IET Renewable Energy Series 6.

[3] H. Saadat, *Power System Analysis*, 2nd ed. New York, NY, USA: McGraw Hill, 2002.

[4] J. A. P. Lopes, C. L. Moreira, and A. G. Madureira, "Defining control strategies for MicroGrids islanded operation," *IEEE Trans. Power Syst.*, vol. 21, pp. 916–924, 2006.

[5] B. Awad, J. Wu, and N. Jenkins, "Control of distributed generation," *Electrotechn. Info. (2008)*, vol. 125/12, pp. 409–414.

[6] J. C. Vasquez, J. M. Guerrero, E. Gregorio, P. Rodriguez, R. Teodorescu, and F. Blaabjerg, "Adaptive droop control applied to distributed generation inverters connected to the grid," in *Proc. 2008 IEEE ISIE*, pp. 2420–2425.

[7] H. Bevrani and S. Shokoohi, "An intelligent droop control for simultaneous voltage and frequency regulation in islanded microgrids," *IEEE Trans. Smart Grid*, vol. 4, no. 3, pp. 1505–1513, Sep. 2013.

[8] J. C. Vasquez, J. M. Guerrero, M. Savaghebi, and R. Teodorescu, "Modelling, analysis and design of stationary reference frame droop controlled parallel three-phase voltage source inverters," in *Proc. 2011 IEEE 8th ICPE & ECCE*, pp. 272–279.

[9] T. L. Vandoorn, B. Meersman, J. D. M. De Kooning, and L. Vandevelde, "Analogy between conventional grid contro and islanded microgrid control based on a global DC-link voltage droop," *IEEE Trans. Power Delivery*, vol. 27, no. 3, pp. 1405–1414, Jul. 2012.

[10] H. Laaksonen, P. Saari, and R. Komulainen, "Voltage and frequency control of inverter based weak LV network microgrid," presented at the Int. Conf. Future Power Syst., Amsterdam, The Netherlands, Nov. 18, 2005.

[11] J. C. Vasquez, R. A. Mastromauro, J. M. Guerrero, and M. Liserre, "Voltage support provided by a droop-controlled multifunctional inverter," *IEEE Trans. Ind. Electron.*, vol. 56, pp. 4510–4519, 2009.

[12] H. Li, F. Li, Y. Xu, D. T. Rizy, and J. D. Kueck, "Adaptive voltage control with distributed energy resources: Algorithm, theoretical analysis, simulation and field test verification," *IEEE Trans. Power Syst.*, vol. 25, pp. 1638–1647, Aug. 2010.

[13] H. Li, F. Li, Y. Xu, D. T. Rizy, and S. Adhikari, "Autonomous and adaptive voltage control using multiple distributed energy resources," *IEEE Trans. Power Syst.*, vol. 28, no. 2, pp. 718–730, May 2013.

[14] L. D. Watson and J. W. Kimball, "Frequency regulation of a microgrid using solar power," in *Proc. 2011 IEEE APEC*, pp. 321–326.

[15] M. G. Molina and P. E. Mercado, "Modeling and control of grid-connected photovoltaic energy conversion system used as a dispersed generator," in *Proc. 2008 IEEE/PES Transm. Distrib. Conf. Expo.: Latin America*, pp. 1–8.

[16] N. Kakimoto, S. Takayama, H. Satoh, and K. Nakamura, "Power modulation of photovoltaic generator for frequency control of power system," *IEEE Trans. Energy Conv.*, vol. 24, pp. 943–949, 2009.

[17] T. Ota, K. Mizuno, K. Yukita, H. Nakano, Y. Goto, and K. Ichiyanagi, "Study of load frequency control for a microgrid," in *Proc. 2007 AUPEC Power Eng. Conf.*, pp. 1–6.

[18] L. Xu, Z. Miao, and L. Fan, "Coordinated control of a solar battery system in a microgrid," in *Proc. 2012 IEEE/PES Transm. Distrib. Conf. Expo. (T&D)*, pp. 1–7.

[19] M. G. Villalva, J. R. Gazoli, and E. R. Filho, "Comprehensive approach to modeling and simulation of photovoltaic arrays," *IEEE Trans. Power Electron.*, vol. 24, no. 5, pp. 1198–1208, 2009.

[20] Y. Xu, H. Li, D. T. Rizy, F. Li, and J. D. Kueck, "Instantaneous active and nonactive power control of distributed energy resources with a current limiter," in *Proc. IEEE Energy Conversion Congr. Expo.*, 2010, pp. 3855–3861.

[21] O. Tremblay and L. A. Dessaint, "Experimental validation of a battery dynamic model for EV applications," *World Electric Vehicle J.*, vol. 3, 2009.

[22] Y. Xu, F. Li, D. T. Rizy, and J. D. Kueck, "Active and nonactive power control with distributed energy resources," in *Proc. 2008 40th North American Power Symp. NAPS'08*, pp. 1–7.

[23] S. Adhikari *et al.*, "Utility-side voltage and PQ control with inverter-based photovoltaic systems," in *Proc. 18th World Congr. IFAC*, Milan, Italy, Aug. 28–Sep. 2 2011, pp. 6110–6116.

Sarina Adhikari (S'08) received the B.E. degree in electrical engineering from Institute of Engineering, Pulchowk Campus, Pulchowk, Lalitpur, Nepal, in 2002 and the M.E. degree in electrical power systems management from Asian Institute of Technology, Pathumthani, Thailand, in 2005. She is currently pursuing the Ph.D. degree in electrical engineering at The University of Tennessee, Knoxville, TN, USA.

Her research interests are voltage stability, distributed energy resources and integration and controls of renewable energy in distribution systems.

Fangxing (Fran) Li (M'01–SM'05) received the Ph.D. degree from Virginia Tech, Blacksburg, VA, USA, in 2001.

He is presently an Associate Professor at The University of Tennessee at Knoxville and the Director of the Education Program of the CURENT research center. He was a principal consulting R&D engineer at ABB Consulting prior to joining UT. His area of interests include distributed energy resources, microgrids, renewable energy integration, power markets and power system computing.

Prof. Li is a registered Professional Engineer in North Carolina, an Editor of IEEE Transactions on Sustainable Energy, and a Fellow of IET.